

Hydrogen in beryllium: Solubility, transport, and trapping

M. G. Ganchenkova,¹ V. A. Borodin,² and R. M. Nieminen¹

¹COMP/Laboratory of Physics, Helsinki University of Technology, P.O. Box 1100, 02015, Espoo, Finland

²RRC Kurchatov Institute, Kurchatov Square 1, 123182 Moscow, Russia

(Received 4 November 2007; revised manuscript received 2 February 2009; published 1 April 2009)

The paper presents the results of *ab initio* simulation of hydrogen properties in beryllium. Both interstitial hydrogen positions in the lattice and various hydrogen positions in a vacancy have been studied. The most energetically favorable interstitial hydrogen configuration among the four considered high-symmetry configurations is the basal tetrahedral one, in agreement with the earlier predictions. The most probable diffusion pathway for hydrogen atoms in the bulk involves the exchange of octahedral and basal tetrahedral positions with the effective migration energy of ~ 0.4 eV. For hydrogen atom in a vacancy, an off-center (nearly basal tetrahedral) configuration is definitely preferred. Addition of more hydrogen atoms to a vacancy remains energetically favorable up to at least five hydrogen atoms, though the binding energies fall down with the increase in the number of hydrogen atoms in the vacancy.

DOI: [10.1103/PhysRevB.79.134101](https://doi.org/10.1103/PhysRevB.79.134101)

PACS number(s): 61.72.J-, 81.05.Bx

I. INTRODUCTION

Hydrogen behavior in metals is a topic of multiple studies due to both the interesting physical phenomena it induces and the practical problems it causes. Among the interesting physical effects one can mention essentially different hydrogen behavior in hcp metals, as compared to bcc and fcc metals. For example, in hcp lattices noticeable amounts of hydrogen stay in solid solution down practically to absolute zero temperatures,¹ whereas solubility of hydrogen in fcc and bcc materials at low temperatures is almost vanishing. Moreover, the low-temperature ordering of hydrogen atoms along the *c* axis seems to be a common effect in various hcp metals.¹⁻³ From the application-relevant point of view, the understanding of hydrogen behavior is required in order to minimize the often detrimental hydrogen effects on metals (e.g., embrittlement)⁴ and to allow the efficient hydrogen use in various energy storage and energy production applications.

During the last decade the experimental studies of hydrogen in metals have been supplemented with computational modeling in order to reveal the atomistic details of hydrogen behavior, such as hydrogen solubility, long range transport, and interaction with the lattice defects. For instance, detailed simulations of hydrogen properties are available for such hcp metals as Y,^{5,6} Zr,⁷ and Mg (Ref. 8); much effort has been put in the study of various rare earths.⁹ In this respect, beryllium remains investigated to extremely limited degree. The only first-principles calculations of hydrogen parameters in Be that we are aware of were presented a decade ago.¹⁰

Meanwhile, beryllium is an advanced material for use in applications requiring lightweight structures. It is also seriously considered as a structural and functional material for future fusion reactors, where it can be highly charged with hydrogen isotopes (deuterium and tritium), through both the direct implantation from the high-temperature plasma and the generation in nuclear transmutation reactions. Hydrogen isotopes are known to be efficiently trapped in beryllium.¹¹⁻¹⁸ The proper understanding of hydrogen properties in beryllium might allow finding of a way to promote

hydrogen release, which would be very beneficial from the technological point of view. First of all, this would allow to decrease the risk of the brittle failure of multigrain beryllium parts during the reactor operation, which results from the accumulation of high anisotropic internal stresses accompanying the hydrogen induced or accelerated cavity formation.^{19,20} Moreover, the released hydrogen, which is generated in Be blanket of fusion reactor in the form of tritium isotope, could be reused in the fuel cycle.

In order to understand the physical mechanisms of hydrogen accumulation and transport in beryllium and to be able to predict the hydrogen effects on beryllium with analytical models (e.g., Ref. 21), one needs to know the basic hydrogen properties, such as the solution energies of hydrogen atoms in different possible interstitial configurations, its migration barriers, the energies of hydrogen binding to vacancies, and other lattice defects (small vacancy complexes, voids, dislocations, etc.). In spite of the multiple experimental studies of hydrogen properties in Be, especially for hydrogen isotopes (deuterium and tritium), the accumulated experimental data are usually characterized by a broad scatter¹⁸ and their reliability is very sensitive to the proper sample handling. For example, the predictions of the typical techniques applied for measurements of hydrogen parameters, such as the thermal desorption spectroscopy (TDS), can be completely misleading if adequate precautions are not taken in order to avoid or minimize the effect of an oxide layer, which blocks hydrogen thermal release. Moreover, the measurement outcome is strongly affected by hydrogen traps created during implantation so that TDS often characterizes hydrogen interaction with traps rather than the parameters of H dissolved in the bulk.

As a result, an accurate determination of hydrogen characteristics in Be remains a challenging task. In particular, the information on hydrogen solubility in Be remains very uncertain and depends very much on whether the sample is charged with hydrogen (or its isotopes) in molecular or atomic atmosphere. According to the most often cited study,²² hydrogen solubility in high purity Be in molecular hydrogen environment demonstrates endothermic heat of solution of 1 eV (see also Ref. 23) at temperatures above

~ 400 °C but no evident temperature dependence at lower temperatures.²² However, other experiments^{24,25} demonstrated no or very weak temperature dependence of hydrogen solubility in the broad temperature range from 300 to 1200 °C [with reported solution activation energies of 0 (Ref. 24) or 0.18 eV (Ref. 25)]. On the other hand, atomic deuterium from a plasma source was found to easily penetrate Be samples with carefully eliminated surface oxide layer.²⁶ Such controversial behavior of hydrogen solubility in Be is often associated with the presence of efficient hydrogen traps. Indeed, TDS experiments indicate the presence of at least two types of deuterium traps with detrapping energies of 1 (Ref. 11) and 1.6–1.8 eV.^{11,27–29} The available experimental data on hydrogen mobility mostly evidence that hydrogen isotopes are fast diffusers in Be, with the experimental estimates for the migration energy of 0.12–0.36 eV,^{23,24,29–32} though a relatively high estimate of 0.77 eV can also be met in the literature.³³

In order to get a better understanding of hydrogen properties at the atomistic level, it is a common practice to use numerical techniques, though the simulations of defects in beryllium are still rare. In particular, Krimmel and Fähnle¹⁰ studied energetic preference of different individual hydrogen atom locations in bulk beryllium and inside a monovacancy and predicted that interstitial hydrogen resides preferentially in basal tetrahedral and octahedral positions, while hydrogen in a vacancy lies in an off-center position in the same basal plane, where the missing atom site is located. As we have recently demonstrated for a monovacancy in Be,³⁴ the sizes of the computational cell used by Krimmel and Fähnle¹⁰ (i.e., 8 to 54 lattice sites for interstitial hydrogen and 36 sites for hydrogen in a vacancy) are too small to provide accurate numbers. Nonetheless, the qualitative predictions of Ref. 10 remain mostly unchanged by the more detailed calculations of this work.

Here we report the results of *ab initio* calculations for hydrogen atoms in both interstitial positions and inside vacancies in a 96-atom beryllium supercell (SC). We also check here a possibility for a monovacancy to collect more than one hydrogen atom, as prompted by an off-center location of individual hydrogen atoms in a vacancy.

II. SIMULATION DETAILS

The calculations in the framework of the density-functional theory (DFT) approach have been performed using VASP code³⁵ with the generalized gradient approximation (GGA), which is known³⁶ to describe the bulk and surface properties of beryllium better than another widespread approximation for exchange-correlation energy: the local density approximation (LDA). Only two electrons per atom were considered explicitly, while the effect of $1s^2$ electrons was represented by ultrasoft Vanderbilt potential implemented in VASP. In the literature one can encounter more sophisticated simulations of Be properties, where all four electrons of Be atom are treated explicitly (e.g., Ref. 37), but we do not expect the explicit treatment of $1s^2$ electrons to notably affect the results, having in mind that the ionization energy of the third electron from Be atom (~ 154 eV) is much higher

than those for $2s^2$ electrons (~ 9.3 and ~ 18.2 eV for the first and the second ones, respectively). During structural optimization, atoms were allowed to relax until the residual forces fell below 0.01 eV/Å³. Brillouin-zone sampling of the wave functions and charge density was done using the gamma-centered Monkhorst-Pack k -point grid.³⁸ The computation cell size, the k -space sampling grid density, and the energy cutoff were selected based on the earlier detailed total cell energy convergence analysis, as described in Ref. 34.

The migration barriers for interstitial hydrogen in the bulk were estimated using the nudged elastic band (NEB) technique,^{39,40} as implemented in VASP, and the drag method.⁴¹ The discussion of weak and strong sides of both techniques can be found in, e.g., Ref. 42, but under proper implementation both should give practically the same barrier values. This was the case also in the current case, though the drag method allowed better profiling of the migration barrier shape than NEB.

Having in mind the necessity to simulate point defect properties, the size of the supercell had to be selected as sufficiently big in order to minimize the interaction of defects with their images, as imposed by periodic boundary conditions. Our earlier calculations for a monovacancy³⁴ demonstrate that the use of small supercells results in quite noticeable overestimation of the vacancy formation energy. On the other hand, in order to reach the total energy convergence in a 96-atom SC with a vacancy, the energy cutoffs of at least 550–600 eV and at least (9,9,9) k -point sampling grid were necessary. Further refinement of the computational output requires the increase in the supercell size up to at least 200 atoms without relaxing the restrictions on the energy cutoff and k -point sampling grid, which presently consumes too much computational resources for a systematic study involving many different defect configurations. As the difference between the converged estimate of the vacancy formation energy and the value obtained for 96-atom SC was less than 0.1 eV,³⁴ here we restrict ourselves to the 96-atomic SC, the energy cutoff of 575 eV, and (9,9,9) k -point sampling grid as a reasonable compromise between the supercell size and the computational efficiency. A check of the sensitivity of configuration energies of two stable configurations of interstitial hydrogen in the bulk (as discussed below) to the k -mesh density (Fig. 1) demonstrates that (9,9,9) k -point sampling is already close to the converged values. The hcp beryllium lattice parameters were selected here the same as in our earlier paper,³⁴ namely, $a=2.259$ Å and $c/a=1.572$.

III. SIMULATION RESULTS

A. Hydrogen atoms in interstitial positions

Assuming that hydrogen atoms occupy high-symmetry positions in the lattice, four well-known interstitial positions are potential candidates for hydrogen atom locations [Fig. 2(a)]. Two of these—tetrahedral (T) and octahedral (O)—are located between the basal planes, while two others—basal tetrahedral (BT) and basal octahedral (BO)—are projections of T and O, respectively, onto a nearby basal plane. All four locations were tested as initial configurations for molecular static relaxation of individual hydrogen atoms.

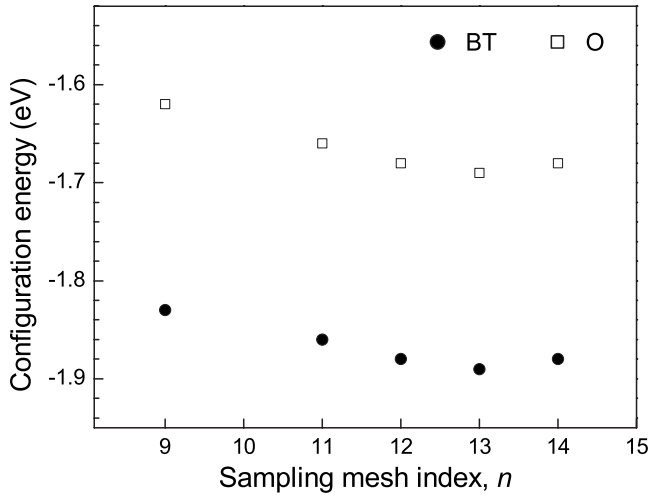


FIG. 1. The configuration energies of hydrogen atoms located in interstitial positions BT and O as a function of the index of (n, n, n) k -point sampling mesh.

Only two of the initial positions turned out to be stable, namely, BT and O. Configuration T was found to reconstruct into BT, while BO reconstructed into O. The stable interstitial hydrogen positions are essentially the same as in Ref. 10. Krimmel and Fähnle¹⁰ proposed one more equilibrium position located 0.02 nm above BT, which was in their calculations the final position for hydrogen atom located initially in T configuration. The latter result seems to be an artifact of the relaxation procedure, related to the flatness of the hydrogen potential energy surface close to BT position [cf. Fig. 3(a)]. In our calculations of T-interstitial relaxation with the standard residual force cutoff of 0.01 eV/Å³ such incomplete relaxation was also met. However, a closer inspection of the residual forces revealed that hydrogen atom had not yet been fully relaxed and with the decrease of the force cutoff it continued to shift toward BT.

Table I shows the calculated hydrogen atom configurational energies E_c^H defined as

$$E_c^H = E_{\text{tot}}^{\text{Be+H}} - E_{\text{tot}}^{\text{Be}}, \quad (1)$$

where $E_{\text{tot}}^{\text{Be+H}}$ and $E_{\text{tot}}^{\text{Be}}$ are the total energies of simulation cells with and without the hydrogen atom. As can be seen, BT configuration is approximately 0.2 eV more energetically fa-

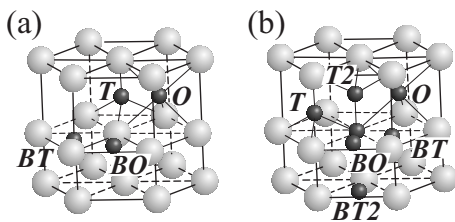


FIG. 2. (a) The high-symmetry positions (marked by small black spheres) in the bulk hcp lattice (shown with light gray spheres) used as initial hydrogen atom locations for molecular static relaxation. (b) Various considered initial hydrogen positions in a vacancy. Hydrogen position on the empty lattice site (C) is not labeled for figure clarity.

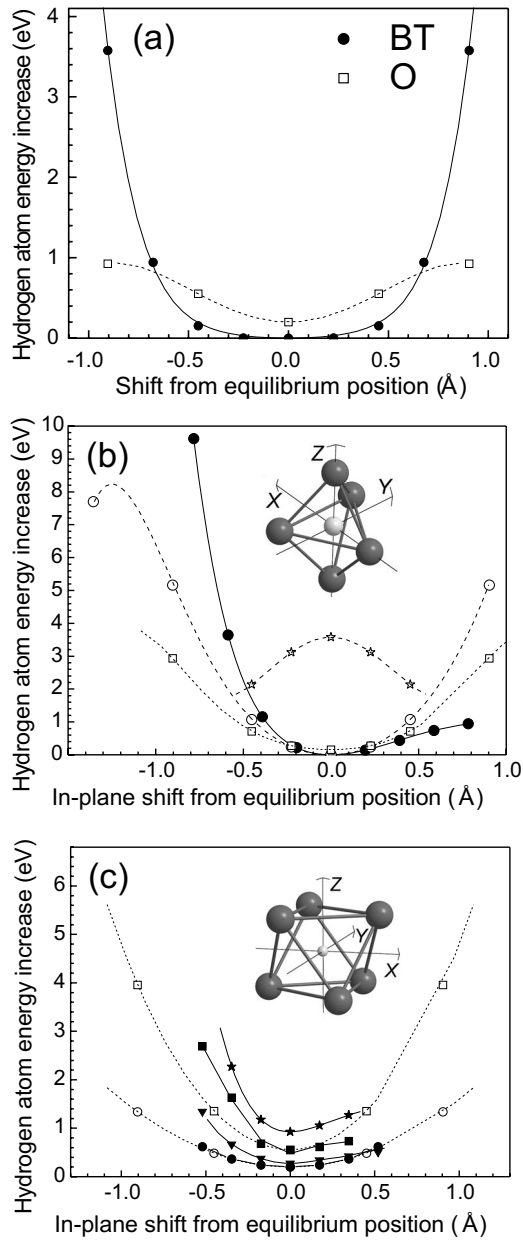


FIG. 3. The shapes of the hydrogen potential surface near the equilibrium positions. (a) U_{BT} and U_O as a function of hydrogen shift along the Z axis. (b) U_{BT} as a function of shifts parallel to the basal plane at different elevations z over the basal plane, as indicated by different symbols: 0 (circles), ~ 0.45 (squares), and ~ 0.9 Å (stars). (c) Same for U_O ; symbol shapes indicate different shifts from O position in Z direction: 0 (circles), ~ -0.22 (triangles), ~ -0.45 (squares), and ~ -0.9 Å (stars). Closed and open symbols in (b) and (c) correspond, respectively, to shifts along X- and Y-coordinate axes, as indicated in the insets for corresponding configurations. All curves are to guide the eyes.

vorable than O. Comparison of this difference with that calculated by Krimmel and Fähnle¹⁰ in smaller size supercells shows quite reasonable agreement (cf. 0.17 eV for 36-atomic and 0.15 eV for 54-atomic supercells).

In addition to the configurational energies, Table I contains estimates of the hydrogen heat of solution in the bulk Be, U_S , which is the activation energy of hydrogen solution

TABLE I. The calculated configurational energy E_c^H and heat of solution U_S of hydrogen in stable interstitial positions in beryllium lattice.

Configuration	E_c^H (eV)	U_S (eV)
BT	-1.82	1.58
O	-1.61	1.79

in a Be sample charged in a constant pressure and temperature hydrogen environment. In such conditions, the temperature dependence of hydrogen solubility, C_S , on temperature T is typically described by the Arrhenian curve,

$$C_S = C_{S0} \exp(-U_S/k_B T), \quad (2)$$

where k_B is the Boltzmann factor and the pre-exponential C_{S0} depends on the environmental hydrogen pressure, the sample surface properties, and possibly on the temperature but only weakly as compared to the exponential contribution. In other words, U_S is the experimentally measurable value, which can be related to the hydrogen atom configurational energy as

$$U_S = E_{\text{tot}}^{\text{Be+H}} - E_{\text{tot}}^{\text{Be}} - E_{\text{ref}}^H = E_c^H - E_{\text{ref}}^H, \quad (3)$$

where E_{ref}^H is the energy of a hydrogen atom outside the sample. For typical experiments, where hydrogen solubility is measured in equilibrium with the high-pressure molecular hydrogen environment, the appropriate reference energy is, evidently, half of the energy of hydrogen molecule or, according to our calculations in the same DFT framework, $E_{\text{ref}}^H = -3.4$ eV.

When assigning the ground-state configuration to interstitial hydrogen atoms, one should not forget that hydrogen is a light element and its total energy can include a non-negligible contribution from zero-point vibrations⁴³ even at zero absolute temperature, as adopted in DFT calculations. According to the estimates of Ref. 10, zero-point vibration energies in interstitial sites for the lightest hydrogen isotope (protium) can reach ~ 0.2 eV and thus do not affect much the absolute values of hydrogen configuration energies or the heat of solution. However, zero-point vibration contributions are comparable in their magnitude to the energy difference between the two equilibrium H configurations. In such situation one cannot *a priori* exclude that zero-point vibration effects would not revert the assignment of the hydrogen ground state (cf., for example, recent calculations for fcc palladium hydride⁴⁴). According to Ref. 10, in beryllium this should not be the case because the zero-point vibration energies in different equilibrium positions differ by less than 0.05 eV even for the lightest hydrogen isotope (protium). However, the latter estimates were made for quite a small cluster (Be_8H) and on unrelaxed Be lattice. So here we have performed a crude estimate of the zero-point vibration contribution to the energies of hydrogen atoms in stable equilibrium positions for our computational outfit.

An accurate calculation of the zero-point hydrogen vibration energies is usually done (see, e.g., Ref. 45) in two steps. First of all, the hydrogen potential surface in the bulk is calculated, typically applying first-principles techniques. At

the second step, the zero-energy vibration energy is estimated by solving the wave equation for hydrogen ion in the obtained potential field. The latter is, generally, quite a complicated task, but in the simplest approximation, neglecting the anharmonicity effects, it is possible to estimate the zero-vibration energies from the curvature of the potential surface at the local energy minima, corresponding to the equilibrium positions. Following this strategy, we have estimated the shape of the hydrogen potential energy surface in the vicinity of BT and O interstitial position. This has been achieved by shifting hydrogen atom from its equilibrium positions along all three Cartesian axes in the fully relaxed 96-site supercells and calculating the total supercell energy for different hydrogen shifts. All beryllium atoms during this procedure were fixed in their relaxed positions, without adiabatic adjustment to shifted hydrogen positions. This simplification seems reasonable because one should care about the zero-point vibration effects only if their contribution to the hydrogen solution energy is sufficiently high, at least ~ 0.1 eV. The latter value would correspond to the zero-point hydrogen atom frequency of ~ 300 THz, which is too fast to be followed by the surrounding beryllium atoms. The calculated output data are presented in Fig. 3.

For BT position the potential energy profile in the c -axis direction varies little up to the shift of ~ 0.6 Å, after which it grows sharply due to the approach to a beryllium atom in the neighboring basal plane. On the other hand, one can hardly expect that hydrogen atom would shift much in the z direction because such a shift involves the reversal of the energy extremum sense from minimum to maximum [cf. curve for $z \approx 0.9$ Å in Fig. 3(b)] and the hydrogen atom would simply drift away from BT position. On the other hand, at smaller z -shifts the whole potential surface can be nicely approximated by polynomials of maximum sixth order for all Cartesian coordinates. In fact, the inclusion of the anharmonic terms is required mostly for the accurate description of potential profile closer to neighboring atoms and saddle points, while for the shifts within 0.3 Å from the BT position the potential, U_{BT} , is nicely fit by purely harmonic function,

$$U_{\text{BT}}(r, z) = U_{\text{BT}}(0) + 4.7r^2 + 0.57z^2, \quad (4)$$

where r and z stand, respectively, for the shifts parallel to the basal plane and normal to it, the distance units are Ångströms, $U_{\text{BT}}(0)$ is the energy of H atom in BT position, and the energies are measured in electron volts.

In contrast to BT, the octahedral position allows unhindered hydrogen movement both in the basal plane and along the c axis. The movement along the c axis is confined within the neighboring basal planes, while the positions on the basal plane (BO) are, in fact, saddle points. As can be seen in Fig. 3(c), the barrier for transition O-BO without the accompanying relaxation of Be atoms is 0.93 eV, which is more than 50% higher than the real migration barrier along this trajectory. For fixed z values, the main contribution to the variation in the potential, U_O , is given by quadratic term, while anharmonic terms are negligible up to in-plane shifts of at least 0.4 Å, though the factors before r^2 depend, naturally, on z .

In the very close vicinity of the equilibrium position the harmonic approximation for the potential is

$$U_o(r, z) = U_o(0) + 1.4r^2 + 2.0z^2, \quad (5)$$

where $U_o(0)$ is the energy of H atom in octahedral position and other notations and units are as in Eq. (4).

Using relations (4) and (5), one easily obtains the estimates for hydrogen zero-point vibration energies. For the lightest isotope, protium, in BT and O positions the resulting values are 0.23 and 0.17 eV, respectively, in agreement with the earlier estimates.¹⁰ For heavier hydrogen isotopes the contribution of zero-point vibrations additionally decreases, e.g., the corresponding values for tritium atoms are 0.13 and 0.1 eV. As can be seen, the account of zero-point vibration energies decreases the energy difference between BT and O positions from 0.2 down to 0.14 eV but does not change the qualitative conclusion that BT position is the ground state for interstitial hydrogen.

The prediction of the BT configuration as the ground-state hydrogen position and the instability of T configuration distinguish beryllium from the other hcp metals, where both experimental (e.g., Refs. 46 and 47) and theoretical^{5–8} estimates indicate that T position is not only stable but is the dominant hydrogen location [except cobalt, where octahedral position is preferred⁴⁸]. On the other hand, octahedral configuration is generally found to be also stable in hcp metals and, like in the case of Be, is only slightly less energetically favorable as compared to the dominant one [by ~ 0.02 – 0.07 eV in Zr,⁷ ~ 0.13 eV in Y,⁵ and ~ 0.17 eV in Mg (Ref. 8)].

The reason for O and BT positions being preferable for hydrogen atom accommodation can be understood when one looks at the electron-density distribution in the vicinity of hydrogen atoms. As can be seen in Figs. 4(a) and 4(b), the positive charge of the hydrogen ion is efficiently screened by the increase of electron density in its immediate vicinity (the complete proton charge compensation is provided by electron density located within a sphere of ~ 0.77 Å radius from H^+ ion for both equilibrium locations) so that hydrogen dissolved in Be lattice looks more like an atom than like a bare proton. A neutral interstitial atom should tend to occupy the biggest available interstitial holes in order to minimize the repulsion from the nearby lattice atoms. From this point of view the location of well-screened proton in octahedral hole looks to be very reasonable. Figure 5(a) demonstrates that even an octahedral hole is insufficient to fully accommodate hydrogen atom, and its insertion into O position is accompanied with the outward relaxation of six neighboring Be atoms. Corresponding increase in the distance between the O position and its Be neighbors constitutes nearly 4.5%. On the other hand, the insertion of hydrogen atom into BT position causes primarily the relaxation of a triangle of its nearest neighbors in the basal plane, which expands by nearly 13% [Fig. 5(b)]. Yet, in spite of such noticeable local lattice distortion, hydrogen in BT position is energetically more favorable than in O position. A possible reason for that can be the fact that the electron density in the bulk Be lattice is noticeably higher in BT positions than anywhere else in the lattice [Fig. 4(c)], and hence the screening of a proton in this posi-

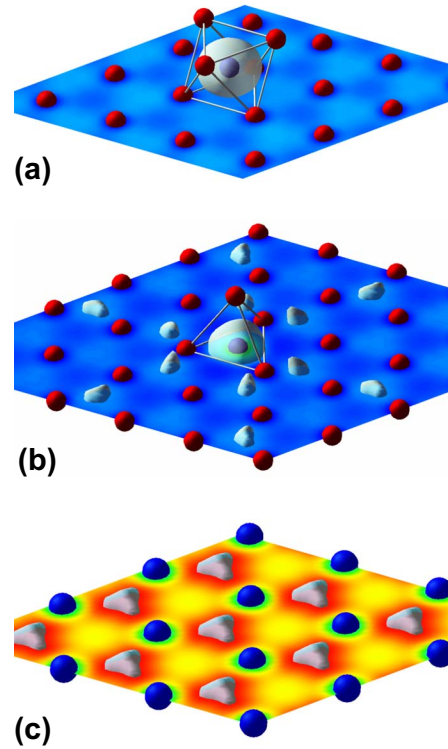


FIG. 4. (Color online) The distribution of electron density near H atom in positions (a) O and (b) BT and in the (c) bulk Be supercell. In order to give a better feeling for hydrogen atom location, the visible nearest neighbors of hydrogen atoms are shown connected with virtual bonds. The planes in each figure show the charge-density distribution within basal planes (in each subfigure the lighter shade means higher electron density; shading intensities of different subfigures are uncorrelated). Also shown are the charge-density isosurfaces corresponding to $0.31e^-/\text{Å}^3$ in (a) and (b) and to $0.29e^-/\text{Å}^3$ in (c).

tion is easier than in locations with low electron density. We thus see that the energetic proficiency of locating hydrogen atom in that or other high-symmetry position is determined by a competition between the repulsion from nearby Be atoms and the electron-density localization.

An interesting feature of the electronic energy distribution around hydrogen atoms in BT configuration [Fig. 4(b)] is the pronounced increase in electronic density in BT positions around H atom in the same basal plane. Having in mind that

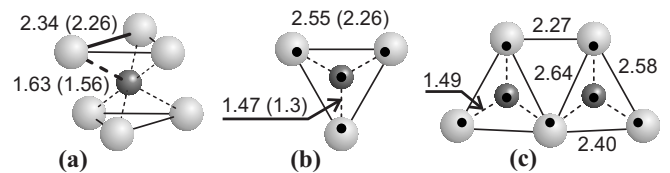


FIG. 5. Lattice relaxation patterns around an interstitial hydrogen atom in positions (a) O and (b) BT and around an interstitial pair in (c) BT positions. Light spheres represent beryllium atoms and small darker spheres—hydrogen atoms. Black points in (b) and (c) denote positions of corresponding lattice sites and BT positions. Numbers at bonds indicate their lengths in relaxed supercells (in Ångströms); numbers in parentheses—the same lengths in the bulk Be supercell.

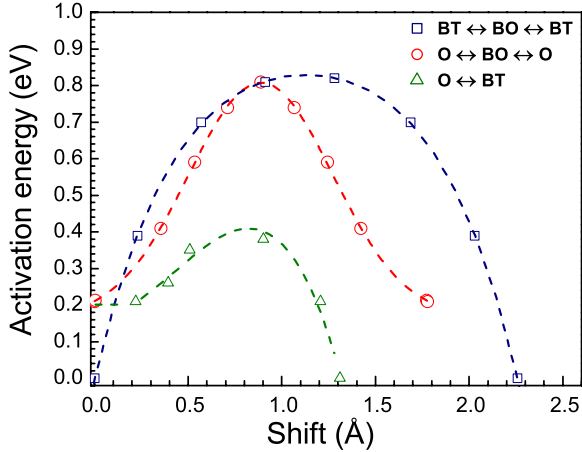


FIG. 6. (Color online) The activation energy profiles for hydrogen jumps between different neighbor positions estimated using the drag method (transition $O \rightarrow O$ along the c axis) or nudged elastic band technique (two other jumps). The shifts are measured as projections of the trajectory points onto the line connecting the starting and the final positions of the jump. The dashed lines are to guide the eyes.

the electron density increase promotes the capture of hydrogen ions, it might be speculated that positioning two hydrogen atoms in neighboring BT positions would result in additional energy gain. Our calculations indicate, however, that this is not the case. Indeed, as can be seen in Fig. 5(c), the elastic distortion of the lattice near a hydrogen pair is more pronounced than in the case of individual hydrogen atoms. As a result, the energy of hydrogen atom pair in the nearby BT positions is 0.17 eV higher than the sum of energies of two isolated hydrogen atoms. In other words, hydrogen atoms in the same basal plane tend to avoid each other. For comparison, according to our calculations a pair of hydrogen atoms in neighboring O and BT positions practically does not interact.

The two equilibrium configurations of a hydrogen atom are such that the most probable jumps are either between neighboring BT and O positions or between two O neighbors along the c axis. Tracing the diffusion jump trajectories with the help of both the nudged elastic band and the drag approaches, we could find that the jump from position O to position BT involved the energy barrier of ~ 0.16 eV, while the reverse barrier is ~ 0.38 eV (Fig. 6). The O-O jump along the c axis is characterized by the energy barrier of ~ 0.6 eV. All the barrier estimates are with respect to the directly calculated hydrogen equilibrium energies and do not take into account possible zero-point energy corrections.

In addition, we have checked a “direct” jump between two nearby BT positions so that the jump trajectory would remain completely in the basal plane. In this case the resulting jump trajectory consisted of two straight segments connecting BT positions with the intervening BO position (a saddle point) and the migration barrier slightly exceeded 0.8 eV. Summing up, the principal migration pathway for a hydrogen atom is the sequence of jumps between BT and O positions with the apparent migration barrier of ~ 0.38 eV. This value nicely correlates with some available experimen-

TABLE II. The calculated hydrogen energies in equilibrium locations inside a vacancy.

Configuration	E_c^{VH} (eV)	E_b^{VH} (eV)
BT	1.51	1.27
T2	1.67	1.12
C ^a	2.67	0.12

^aUnstable equilibrium.

tal data, e.g., with the migration barrier value of 0.36 eV measured in Refs. 23 and 30.

The dominant hydrogen migration mechanism in Be looks to be very similar to that predicted for other hcp metals, where diffusion jumps follow preferentially the T-O-T trajectory. Even the calculated hydrogen migration barriers are very similar to those we find for Be, namely, ~ 0.41 [Zr (Ref. 7)] and ~ 0.46 eV [Y (Ref. 5)] for jumps from T to neighboring O site and ~ 0.7 eV [Zr (Ref. 7)] and ~ 0.85 eV [Y (Ref. 5)] for direct O-O jumps along the c axis. These calculated values are in good agreement with the experimental estimates for activation energy of hydrogen diffusion in Zr and Y, which demonstrate notably less scattering than in beryllium.

In estimating the hydrogen mobility it should be remembered that the classical expression for the diffusion coefficient in terms of Arrhenian temperature dependence is valid only for temperatures above approximately half the Debye temperature, while at the lower temperatures quantum corrections noticeably influence hydrogen mobility.⁴⁹ The Debye temperature for beryllium is quite high and so the quantum corrections can be neglected only above ~ 200 °C, which, however, can be relevant e.g. for the operation of beryllium components of fusion reactors.

B. Hydrogen atom in a vacancy

According to earlier predictions,¹⁰ vacancies in Be are efficient traps for hydrogen atoms. Indeed, a hydrogen atom on an interstitial position causes noticeable elastic strain in the surrounding lattice. The energy of elastic relaxation can be essentially decreased when the hydrogen atom is placed in a relatively big hole provided by a vacancy (in what follows we mean by vacancy the empty space up to the first nearest neighbors of the vacant site rather than the vacant site itself). In this study we have relaxed a hydrogen atom starting from seven initial positions, as shown in Fig. 2(b). Mostly these positions are the same as in the bulk, and thus nearly the same notation is used. The additional positions arise because (i) some of the positions that were equivalent in the bulk are no more equivalent in the vicinity of the vacant site and (ii) the hydrogen atom can occupy the vacant site itself (C position).

The resulting final configuration energies of hydrogen atoms and their binding energies to the vacancy are summarized in Table II. The binding energy of hydrogen atom is defined here as compared to its most energetically favorable position in the bulk,

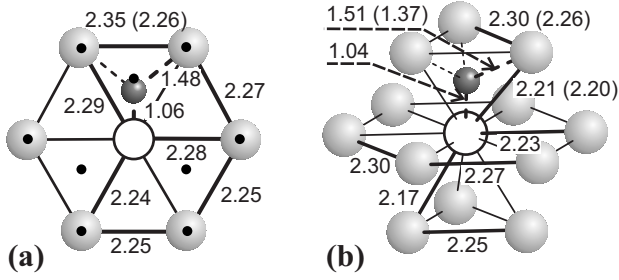


FIG. 7. Lattice relaxation patterns around a hydrogen atom in positions (a) BT and (b) T2 inside a vacancy. In case of BT configuration only relaxation in the basal plane is shown. The marked bonds are emphasized by thicker lines; other notation is like in Fig. 5.

$$E_b^{VH} = E_{\text{tot}}^{\text{Be+H}} + E_{\text{tot}}^{\text{Be+V}} - E_{\text{tot}}^{\text{Be}} - E_{\text{tot}}^{\text{Be+VH}} = E_c^{\text{H}} + E_c^{\text{V}} - E_c^{\text{VH}}, \quad (6)$$

where $E_{\text{tot}}^{\text{Be+X}}$ and E_c^{X} are, respectively, the total energy of the beryllium supercell with the defect and the defect configurational energy; X denotes here the defect configuration: interstitial hydrogen in BT position ($X=H$), an isolated vacancy ($X=V$), and a hydrogen atom inside the vacancy ($X=VH$). The configurational energy of the vacancy for the same computation parameters as those used here, $E_c^{\text{V}} = 4.6$ eV, has been calculated in our previous work.³⁴

Only two of the considered positions were found to correspond to the local energy minima, namely, BT and T2, with BT being ~ 0.15 eV more favorable. The fact that hydrogen atom in a vacancy is located in an off-center (BT) position agrees with the earlier predictions.¹⁰ Hydrogen atom in the octahedral position is, in contrast to the bulk, unstable and relaxes to the nearby T2. Configurations BO and BT2 also relax to a nearby T2, while T relaxes into BT. Hydrogen located initially exactly on the vacant site (configuration C) did not move from its original position during the lattice relaxation run, but this was only due to its high symmetry. The C-configuration energy is nearly 1.2 eV higher than that of BT configuration and the equilibrium is unstable. In fact, a small shift of hydrogen atom from C position sufficed to promote its relaxation toward the nearest energy minimum.

It is interesting to compare the electron-density distribution in a vacancy and the lattice relaxation around equilibrium H positions inside vacancy with those for a pure vacancy in the bulk. The elastic relaxation pattern of V-H complex, as shown in Fig. 7, demonstrates a clear qualitative difference from that around a pure vacancy (cf. Fig. 4 in Ref. 34). While the neighboring atoms of a pure vacancy shift slightly toward the empty site, the addition of a hydrogen atom in either BT or T2 position changes the elastic relaxation close to the hydrogen atom to the outward one. Note also that in the case of axially symmetric T2 configuration the symmetry of the atomic ring around the vacancy in the basal plane decreases to C_3 , like for a hydrogen-free vacancy.³⁴

As can be seen in Fig. 8(a), the electronic density distribution inside a vacancy in the bulk Be demonstrates well-pronounced depletion in the center of the vacancy, which

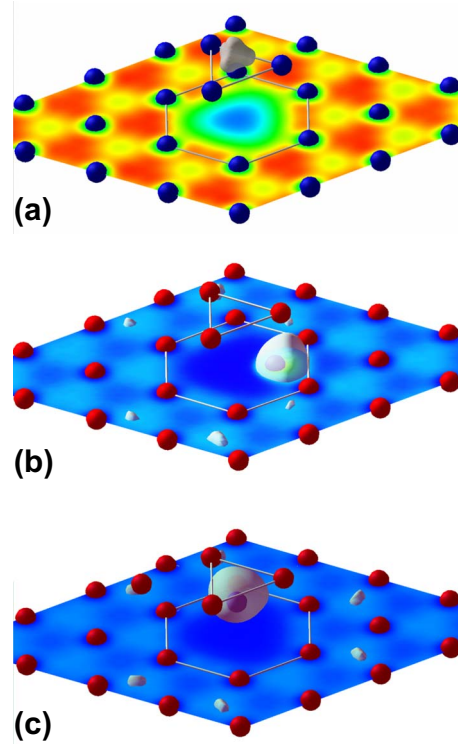


FIG. 8. (Color online) The distribution of electron density near a vacancy in the (a) bulk supercell and in the V-H complex with H atom located in (b) BT and (c) T2 positions. All figures show the charge-density distribution in the basal plane containing the vacancy. In order to better specify the location of the empty lattice site, its six neighbors in the basal plane are connected by bonds and, additionally, three atoms immediately above the vacancy are shown (also connected by bonds). The coloring is such that the darker shade means lower electron density. Also shown are the electron charge-density isosurfaces near the vacant site; all correspond to the density level of $0.3e^{-}/\text{\AA}^3$.

means that the central part of a vacancy is not an attractive place for a proton. On the other hand, the hydrogen atom shift toward the vacant site (by $\sim 20\%$ and $\sim 24\%$ of ideal distances from a lattice site to nearby BT and T2 positions, respectively) decreases the elastic energy associated with the lattice relaxation near hydrogen atoms. As a result, the competition of the electronic and elastic contributions to the hydrogen atom energy keeps the hydrogen atoms at the periphery of the vacancy volume. Note also the asymmetric distribution of electron charge density around hydrogen atoms, where the “center of mass” of the electron cloud around the hydrogen ion is shifted away from the vacant site [Figs. 8(b) and 8(c)].

Finally, it can be seen in Fig. 8 that the vacancy presence increases the electron density in some positions in the immediate vicinity of the vacancy, in particular in two tetrahedral interstitial sites located on the c axis passing through the vacancy and, to a lesser extent, in BT positions in the basal planes neighboring to the basal plane with the vacancy.

C. Several hydrogen atoms in a vacancy

The preferential location of hydrogen atom in an off-center position implies that when a vacancy captures a hy-

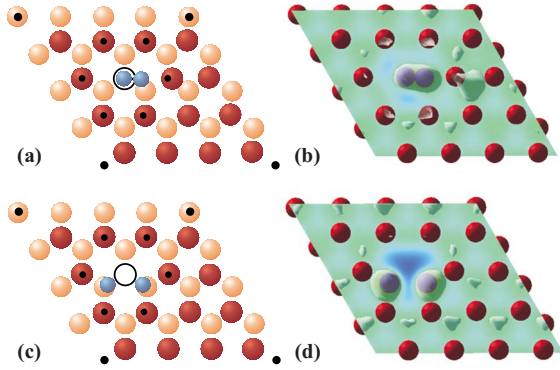


FIG. 9. (Color online) (a) and (b) The close-to-initial and (c) and (d) final states of *ab initio* relaxation of H_2 molecule in a vacancy (view along the c axis). (a) and (c) show the initial and relaxed atomic positions. Darker (red) big spheres depict Be atoms in the basal plane of the vacancy, lighter (red) spheres depict atoms in the basal plane below that of the vacancy, and smaller (blue) spheres depict hydrogen atoms. Black points indicate supercell corners (bigger) and ideal lattice sites near the vacancy (smaller). (b) and (d) represent the corresponding distributions of electron charge density in the basal plane containing the vacancy and isosurfaces of charge density near the basal plane (at the level of $0.3e^-/\text{\AA}^3$).

drogen atom, there remains still plenty of room to accommodate more hydrogen. Hence, we have studied a situation, where several hydrogen atoms are located inside one vacancy.

Where a second hydrogen atom is added to a vacancy, one would wonder whether these two hydrogen atoms form a chemically bound molecule. Our calculations demonstrate that this does not happen. Indeed, when a hydrogen molecule was positioned close to the center of the vacancy, it dissociated into two separate hydrogen atoms. As can be seen in Fig. 9, the region of increased electronic density (chemical bond) between hydrogen atoms, which is easily detectable at the initial stages of relaxation, completely vanishes in the final picture.

The vacancy volume encompasses three BT and two T2 positions, and hence one might expect up to five hydrogen atoms to be accommodated inside a vacancy. According to our calculations, this is indeed the case, though with the increase in the number n of hydrogen atoms their binding energies to the complex defined as

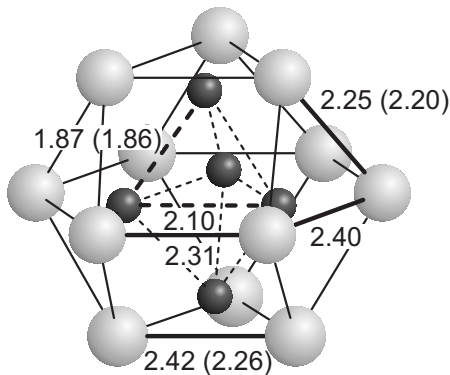


FIG. 10. Lattice relaxation around the complex VH_5 . Notation as in Fig. 5.

TABLE III. The calculated configurational energies of VH_n ($n=2-5$) complexes and hydrogen binding energies to the complex.

n	Configuration	$E_c^{VH_n}$ (eV)	$E_b^{VH_n}$ (eV)
2	2 BT	-1.39	1.08
2	BT+T2	-1.1	0.79
2	2T2	-1.07	0.93
3	3 BT	-4.13	0.92
3	2 BT+T2	-3.98	0.77
4	3 BT+T2	-6.66	0.71
4	2 BT+2 T2	-6.34	0.54
5	3 BT+2 T2	-8.9	0.42

$$E_b^{VH_n} = E_c^H + E_c^{VH_{n-1}} - E_c^{VH_n}, \quad (7)$$

where $E_c^{VH_n}$ is the configuration energy of VH_n complex, fall down. The configuration energies of VH_n complexes and hydrogen binding energies are summarized in Table III. In cases where the removal of a hydrogen atom from VH_n complex is possible from either of two nonequivalent positions, the lowest binding energy is cited. Judging from the energy gain point of view, hydrogen atoms occupy first of all the BT positions and only afterwards the remaining T2 positions.

The accumulation of several hydrogen atoms in a vacancy changes its relaxation pattern from slightly inward to pronouncedly outward, as shown in Fig. 10 for VH_5 . It is interesting, however, that the shifts of vacancy nearest-neighbor atoms occur primarily within their own basal planes, whereas deviations along the c axis remain within 0.02 Å even for the biggest complex VH_5 .

The electron charge-density distributions around H ions in complexes VH_n are, like for V-H, asymmetric and shifted from the vacant site (Fig. 11). It can be also seen that the increase in the number of hydrogen atoms in the vacancy is accompanied with noticeable redistribution of electron charge density outside the vacancy. In the case of VH_5 the size of the redistribution zone is comparable with the supercell size, which implies the interaction of the complex with the images in the neighboring supercells. Due to this interaction, the 96-atomic supercell may not provide converged predictions for the biggest VH_n complexes and the quantitative values obtained here for these complexes should be considered with certain caution.

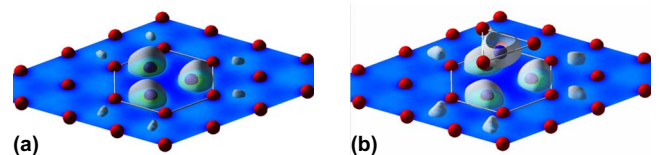


FIG. 11. (Color online) The distribution of electron density near complexes (a) VH_3 and (b) VH_5 . The charge-density isosurfaces correspond to $0.31e^-/\text{\AA}^3$. Also shown are the charge densities in the basal planes containing the vacancies. In both figures the six vacancy neighbors are connected by bonds. In addition, (b) includes three vacancy neighbors located in the plane above the vacancy (these atoms are also connected by bonds).

IV. DISCUSSION

Several findings of the paper are worth discussing. Let us address, first of all, the behavior of hydrogen dissolved in the bulk. Even the lowest calculated heat of solution, ~ 1.6 eV in BT position, is quite large, even forgetting the additional contribution from the zero-level hydrogen vibrations. On the one hand, this agrees well with the results of Ref. 25, showing that hydrogen has a very low solubility in beryllium. On the other hand, the estimated heat of solution is noticeably larger than both the earlier *ab initio* estimate of 0.8 eV (Ref. 10) and the often cited experimental value of 1 eV, as measured by Swansiger.²²

The reasons for the discrepancy between our results and the earlier computations are hard to clarify since neither hydrogen configuration energy nor hydrogen reference state are cited in Ref. 10. But the experimental value is conspicuously similar to one of the well-known hydrogen detrapping energies, as determined by TDS (see Sec. I). This gives a strong hint that the measured value corresponds not to hydrogen dissolved in the matrix but rather to that trapped in vacancies. Correspondingly, instead of Eq. (2), the hydrogen solubility in the matrix is given by

$$C_S = C_{S0} C_V \exp[-(\bar{E}_c^{V-H} - E_c^V - \bar{n}E_{\text{ref}}^H)/k_B T], \quad (8)$$

where \bar{E}_c^{V-H} is the average configuration energy of vacancy-hydrogen complexes and \bar{n} is the average number of hydrogen atoms in a vacancy. If the majority of such complexes contains only one hydrogen atom, then, taking the lowest configuration energy of VH complex (1.51 eV; see Table II), we get $\bar{E}_c^{V-H} - E_c^V - E_{\text{ref}}^H \approx 0.3$ eV. In the case where VH_2 complexes dominate, the latter estimate falls down to 0.2 eV (see Table III). On the other hand, the domination of VH_3 complexes would require already 1.4 eV, so in the kinetic equilibrium of beryllium samples with the hydrogen environment one can hardly expect to charge a vacancy by more than two hydrogen atoms, regardless of the fact that it is able to accommodate up to five.

In other words, where the vacancies are created in a non-thermal way (e.g., quenched in from higher temperatures), the heat of solution is very low (~ 0.2 – 0.3 eV), which provides a possible explanation for the experimental observations of weak temperature dependence of hydrogen solubility (e.g., in Ref. 22 at temperatures below 350 °C). On the other hand, the vacancy formation energy in Be, $E_f^V \sim 0.8$ eV, is sufficiently low to enable noticeable thermal vacancy concentrations at elevated temperatures. In the temperature range where thermal vacancies dominate, the apparent heat of hydrogen solution will include also the contribution from the vacancy formation energy,

$$U_s = \bar{E}_c^{V-H} - E_c^V - \bar{n}E_{\text{ref}}^H + E_f^V \approx 1 \text{ eV}, \quad (9)$$

in excellent agreement with the experimental value observed in Ref. 22 in the high-temperature region (450–510 °C).

The next interesting prediction from the current calculations is that the maximum binding energy of a hydrogen atom with a vacancy is ~ 1.3 eV, provided that the zero-vibration contributions to hydrogen energy are omitted. The

earlier estimates predict somewhat higher value [1.62 eV (Ref. 10)], but the largest part of the difference seems to be due to the inclusion in Ref. 10 of zero-vibration contribution to the hydrogen energy in the bulk (in our case this would give the binding energy of ~ 1.5 eV). However, having in mind that the center of vacancy is a well-pronounced maximum of hydrogen energy, one can expect that the hydrogen potential surface profile in BT positions inside the vacancy is not much different from that in BT position in the bulk. In this case the zero-vibration contributions from these local minima should largely compensate each other in the binding energy calculation and so, in the absence of detailed calculations, it seems safer to omit the zero-vibration contributions to hydrogen-vacancy binding energies altogether.

In any case, the difference between the current and the earlier predictions of H - V binding energy is not really large, though it still might have implications for the interpretation of TDS results. As already discussed in Sec. I, TDS experiments indicate the presence of at least two types of deuterium traps in preimplanted beryllium. The detrapping energy of 1 eV corresponds to a sharp desorption peak, which is most probably associated with a unique trapping center, whereas the relatively broad peak corresponding to detrapping energies of 1.6–1.8 eV is usually assumed to be due to a spectrum of trapping centers with similar trapping efficiencies.^{11,27–29} In terms of these views, the binding energy value of Krimmel and Fähnle¹⁰ associates vacancy-hydrogen complex with the broad peak. With the lower binding energy calculated in this work, it might be more reasonable to associate vacancies containing one to two hydrogen atoms with the sharp peak. This would also agree with the well-known fact that deuterium implanted in beryllium can be retained in atomic and molecular forms,¹⁶ which, according to both our results and earlier considerations,^{11,13,14} corresponds to hydrogen capture in, respectively, monovacancies and voids.

Finally, our calculations have demonstrated that several (at least five) hydrogen atoms can be accommodated in a monovacancy, which indicates that vacancies in beryllium are efficient hydrogen traps. It should be mentioned that accommodation of multiple hydrogen atoms in a vacancy is not a specific feature of beryllium and has been earlier observed^{50,51} and predicted by *ab initio* calculations^{52,53} in a number of metals. The consequences of H-vacancy binding are twofold. First of all, it stabilizes vacancies and can result in an orders of magnitude increase in HV-complex concentrations as compared to the vacancy thermal equilibrium ones. In turn, the superabundant vacancy formation provides more trapping sites for H impurities, effectively increasing the apparent H solubility. As a result, extremely high concentrations of hydrogen can be retained in Be.

Indeed, in an experiment where Be was charged with atomic deuterium from a plasma source, deuterium concentrations of 5–7 at. % were reached²⁶ instead of typical 1–10 ppm for beryllium loaded in molecular hydrogen environment.¹⁸ This result can be easily rationalized if we replace in Eqs. (3) and (9) the reference hydrogen energy E_{ref}^H for molecular hydrogen with that for atomic one. The latter is higher by half the dissociation energy of H_2 molecule, which is predicted by VASP code to be ~ 4.6 eV [cf. experimental

value of 4.75 eV (Ref. 54)], and the heat of atomic hydrogen solution becomes exothermic. In this situation, the solubility of hydrogen is limited only by the number of available vacancies. But, as discussed above, at sufficiently high temperatures (740 K in case of Ref. 26), where thermal vacancies are produced easily, the vacancy stabilization by hydrogen atoms makes accumulation of high vacancy concentrations quite a simple task. It is interesting to mention that Sharapov *et al.*²⁶ emphasized that in their experiment hydrogen traps are produced during the saturation to high deuterium levels and do not require additional sources (such as radiation damage created by implantation).

V. SUMMARY

The results of *ab initio* calculations of hydrogen atoms in beryllium bulk and in a vacancy in Be allow us to make the following conclusions:

(1) the most energetically favorable interstitial hydrogen configuration is the basal tetrahedral (BT) one, with the calculated heat of solution of 1.57 eV. Hydrogen atom in octahedral (O) configuration is 0.2 eV less profitable. The account of zero-point vibrations of hydrogen in equilibrium positions somewhat decreases the difference (to ~ 0.14 eV) but does not change the qualitative picture. Other high-symmetry configurations are unstable and relax to either BT or O, in agreement with the earlier *ab initio* predictions.¹⁰

(2) The most probable diffusion pathway of hydrogen in the bulk involves consecutive jumps between nearby BT and O interstitial positions with apparent migration barrier of ~ 0.38 eV.

(3) A hydrogen atom in a vacancy prefers an off-center configuration close to BT position but shifted by $\sim 20\%$ toward the empty site. Additionally, hydrogen atoms have

metastable configurations close to tetrahedral positions above and below the vacant site, which are ~ 0.15 eV less profitable than BT configurations. Position in the vacancy center is an unstable equilibrium with rather high energy (~ 1.2 eV bigger than in BT).

(4) At least five hydrogen atoms can be captured in a vacancy with positive binding energies, though the binding efficiency falls down with the increase in the number of hydrogen atoms in the vacancy.

(5) The often cited value of 1 eV for the hydrogen heat of solution²² is interpreted here as that corresponding to hydrogen trapping in thermal vacancies rather than to its solution in the bulk. Moreover, where vacancy concentration in the sample is temperature independent, utterly weak temperature dependence of hydrogen solubility is predicted, as in some experimental observations.

(6) It is found that hydrogen solubility in Be is sensitive to the type of gaseous environment during the sample charging, being endothermic for molecular hydrogen environment but exothermic for the atomic one. This provides an explanation of the experimentally observed several orders of magnitude difference in hydrogen solubility in Be loaded in molecular and atomic hydrogen environments.

ACKNOWLEDGMENTS

We are thankful to P. V. Vladimirov (Karlsruhe Institute of Technology), who has drawn our attention to a possible correlation between stable hydrogen positions and the local increases of electronic density in the lattice. The research has been supported in part by the Academy of Finland through the Centers of Excellence program (2006–2011) and through Grant No. SA120004, and by the Russian Foundation for Basic Research through Grant No. 08-08-00603. We also wish to thank the Center for Scientific Computing (Helsinki, Finland) for the use of their computational facilities.

¹J. E. Bonnet, C. Juckum, and A. Lucasson, *J. Phys.F: Met Phys.* **12**, 699 (1982).

²I. S. Anderson, J. J. Rush, T. Udovich, and J. M. Rowe, *Phys. Rev. Lett.* **57**, 2822 (1986).

³M. W. McKergow, D. K. Ross, J. E. Bonnet, I. S. Anderson, and O. Schaerpf, *J. Phys. C* **20**, 1909 (1987).

⁴*Hydrogen in Metals II, Topics in Applied Physics*, edited by J. Völkl and G. Alefeld (Springer, Berlin, 1978), Vol. 29.

⁵J. Michel, J. R. Niklas, and J. M. Spaeth, *Phys. Rev. B* **40**, 1732 (1989); B. J. Min and K. M. Ho, *Phys. Rev. B* **45**, 12806 (1992).

⁶Y. Wang and M. Y. Chou, *Phys. Rev. B* **49**, 13357 (1994).

⁷C. Domain, R. Besson, and A. Legris, *Acta Mater.* **50**, 3153 (2002).

⁸F. Óskarsson, W. Stier, and H. Jónsson (unpublished).

⁹P. Vajda, in *Handbook on the Physics and Chemistry of Rare Earths, Hydrogen in Rare Earth Metals Including RH₂+xPhases*, edited by K. A. Gschneider and L. R. Eyring (Elsevier Science, Amsterdam, 1995), Vol. 20, p. 207.

¹⁰H. Krimmel and M. Fähnle, *J. Nucl. Mater.* **231**, 159 (1996); **255**, 72 (1998).

¹¹W. R. Wampler, *J. Nucl. Mater.* **122-123**, 1598 (1984).

¹²H. Kawamura, E. Ishituka, A. Sagara, K. Kamada, H. Nakata, M. Saito, and Y. Hutamura, *J. Nucl. Mater.* **176-177**, 661 (1990).

¹³W. R. Wampler, *J. Nucl. Mater.* **196-198**, 981 (1992).

¹⁴V. N. Chernikov, V. Kh. Alimov, A. V. Markin, and A. P. Zakharov, *J. Nucl. Mater.* **228**, 47 (1996).

¹⁵N. Yoshida, S. Mizusawa, R. Sakamoto, and T. Muroga, *J. Nucl. Mater.* **233-237**, 874 (1996).

¹⁶V. Kh. Alimov, V. N. Chernikov, and A. P. Zakharov, *J. Nucl. Mater.* **241-243**, 1047 (1997).

¹⁷A. A. Haasz and J. W. Davis, *J. Nucl. Mater.* **241-243**, 1076 (1997).

¹⁸R. A. Causey, *J. Nucl. Mater.* **300**, 91 (2002).

¹⁹V. P. Chakin, V. A. Kazakov, R. R. Melder, Yu. D. Goncharenko, and I. B. Kupriyanov, *J. Nucl. Mater.* **307-311**, 647 (2002).

²⁰L. L. Snead, *J. Nucl. Mater.* **326**, 114 (2004).

²¹M. A. Lomidze, A. E. Gorodetsky, and A. P. Zakharov, *Fusion Technol.* **28**, 1211 (1995).

²²W. A. Swansiger, *J. Vac. Sci. Technol. A* **4**, 1216 (1986).

²³R. G. Macaulay-Newcombe and D. A. Thompson, *J. Nucl. Mater.* **212-215**, 942 (1994).

²⁴P. M. S. Jones and R. Gibson, *J. Nucl. Mater.* **21**, 353 (1967).

- ²⁵V. I. Shapovalov and Y. M. Dukel'skii, *Izv. Akad. Nauk SSSR, Met.* **1988**, 201 [Russ. Metall. **1988**, 210].
- ²⁶V. M. Sharapov, L. E. Gavrilov, V. S. Kulikauskas, and A. V. Markin, *J. Nucl. Mater.* **233-237**, 870 (1996).
- ²⁷R. A. Anderl, M. R. Hankins, G. R. Longhurst, R. G. Pawelko, and R. G. Macaulay-Newcombe, *J. Nucl. Mater.* **196-198**, 986 (1992).
- ²⁸R. Boivin and B. Terreault, *J. Nucl. Mater.* **187**, 117 (1992).
- ²⁹D. Kéroack and B. Terreault, *J. Nucl. Mater.* **212-215**, 1443 (1994).
- ³⁰E. Abramov, M. P. Riehm, and D. A. Thompson, *J. Nucl. Mater.* **175**, 90 (1990).
- ³¹D. L. Baldwin and M. C. Billone, *J. Nucl. Mater.* **212-215**, 948 (1994).
- ³²I. L. Tazhibaeva, V. P. Shestakov, E. V. Chikhray, O. G. Romanenko, A. Kh. Klepikov, G. L. Saksaganskiy, Yu. G. Prokofiev, and S. N. Mazaev, in *Fusion Technology, 1994: Proceedings of The 18th Symposium on Fusion Technology*, Karlsruhe, Germany, 22–26 August 1994 (North-Holland, Amsterdam, 1995), p. 427.
- ³³R. P. Doerner, A. Grossman, S. Luckhardt, R. Seraydarian, F. C. Sze, D. G. Whyte, and R. W. Conn, *J. Nucl. Mater.* **257**, 51 (1998).
- ³⁴M. G. Ganchenkova and V. A. Borodin, *Phys. Rev. B* **75**, 054108 (2007).
- ³⁵G. Kresse and J. Hafner, *Phys. Rev. B* **47**, 558 (1993); G. Kresse and J. Furthmüller, *ibid.* **54**, 11169 (1996).
- ³⁶N. A. W. Holzwarth and Y. Zeng, *Phys. Rev. B* **51**, 13653 (1995).
- ³⁷G. Robert and A. Sollier, *J. Phys. IV France* **134**, 25 (2006).
- ³⁸H. J. Monkhorst and J. D. Pack, *Phys. Rev. B* **13**, 5188 (1976).
- ³⁹H. Jonsson, G. Mills, and K. W. Jacobsen, in *Classical and Quantum Dynamics in Condensed Phase Simulations*, edited by B. J. Berne, G. Ciccotti, and D. F. Coker (World Scientific, Singapore, 1998), p. 385.
- ⁴⁰G. Henkelman and H. Jonsson, *J. Chem. Phys.* **113**, 9978 (2000).
- ⁴¹R. Johnson and J. Beeler, in *Interatomic Potentials and Crystal-line Defects*, edited by J. K. Lee (The Metallurgical Society of AIME, Warrendale, PA, 1981), p. 165.
- ⁴²V. A. Borodin and M. G. Ganchenkova, in *Handbook of Theoretical and Computational Nanotechnology*, edited by M. Rieth and W. Schommers (American Scientific, Stevenson Ranch, CA, 2006), Vol. 5, p. 437.
- ⁴³N. W. Ashcroft and N. D. Mermin, *Solid State Physics* (Holt, Rinehart and Winston, New York, 1976).
- ⁴⁴M. Dyer, C. Zhang, and A. Alavi, *ChemPhysChem* **6**, 1711 (2005).
- ⁴⁵C. Elsässer, K. M. Ho, C. T. Chan, and M. Fähnle, *Phys. Rev. B* **44**, 10377 (1991).
- ⁴⁶D. Khatamian, C. Stassis, and B. J. Beaudry, *Phys. Rev. B* **23**, 624 (1981).
- ⁴⁷J.-W. Han, C.-T. Chang, D. R. Torgeson, E. F. W. Seymour, and R. G. Barnes, *Phys. Rev. B* **36**, 615 (1987).
- ⁴⁸V. K. Fedotov, V. E. Antonov, T. E. Antonova, E. L. Bokhenkov, B. Dorner, G. Grosse, and F. E. Wagner, *J. Alloys Compd.* **291**, 1 (1999).
- ⁴⁹C. P. Flynn and A. M. Stoneham, *Phys. Rev. B* **1**, 3966 (1970).
- ⁵⁰Y. Fukai and N. Okuma, *Phys. Rev. Lett.* **73**, 1640 (1994).
- ⁵¹Y. Fukai, *Phys. Scr.*, T **103**, 11 (2003).
- ⁵²Y. Tateyama and T. Ohno, *Phys. Rev. B* **67**, 174105 (2003).
- ⁵³G. Lu and E. Kaxiras, *Phys. Rev. Lett.* **94**, 155501 (2005).
- ⁵⁴K. P. Huber, G. Herzberg, *Molecular Spectra and Molecular Structure IV. Constants of Diatomic Molecules* (Van Nostrand Reinhold, New York, 1979).